Modeling Thermochemical Nonequilibrium with the Continuous Galerkin Finite Element Flow Solver PHASTA

Connor W. Morency* and Kenneth E. Jansen†
University of Colorado Boulder, Boulder, CO, 80309, USA

This paper aims to introduce developments within the PHASTA flow solver that are needed for applications in hypersonic CFD research. The PHASTA formulation is described and unit tests are performed that serve to validate new features that enable the simulation of thermochemical nonequilibrium. These features include a multi-species reacting flow module, a two-temperature formulation that includes a model for vibrational temperature, a model for mass diffusion, and the Spalart-Allmaras RANS turbulence model. The code accurately predicts the physics for simple problems but requires further development for more complex flows that represent real-world engineering problems.

I. Nomenclature

C_p^{tr}	=	specific heat at constant pressure for the translational-rotational mode, $J/kg/K$
e^{tot}	=	specific total energy, J/kg
e^v	=	specific vibrational energy, J/kg
e_s^v	=	specific vibrational energy of species s, J/kg
h_s	=	specific enthalpy of species s, J/kg
J_{si}	=	diffusion mass flux of species s in the ith direction, $kg/m^2/s$
P	=	pressure, Pa
Q_{c-v}	=	source of vibrational energy due to chemical reactions, $J/m^3/s$
Q_{tr-v}	=	source of vibrational energy due to relaxation via inter-molecular collisions, $J/m^3/s$
q_i	=	heat flux in the ith direction, $J/m^2/s$
q_i^v	=	vibrational heat flux in the ith direction, $J/m^2/s$
R_s	=	specific gas constant of species s, $J/kg/K$
T	=	temperature, K
T^v	=	vibrational temperature, K
u_i	=	velocity in the ith direction, m/s
δ^*	=	displacement thickness of the boundary layer, mm
δ_{ij}	=	Kronecker delta
κ_{tr}	=	thermal conductivity of the translational-rotational mode, $J/s/m/K$
Ω_s	=	mass production rate of species s, $kg/m^3/s$
ρ_s	=	density of species s, kg/m^3
τ_s	=	vibrational relaxation time of species s, s
τ_{ij}	=	viscous stress tensor, $kg/m^2/s^2$
μ_s	=	chemical potential of species s, J/kg
θ	=	momentum thickness of the boundary layer, mm
θ_s^v	=	characteristic vibrational temperature of species s, K

II. Introduction

From cutting-edge incognito spy planes, to the threat of nuclear warheads from overseas, to the dawn of the golden age of space travel, all of these news-worthy phenomena share one thing in common: the vehicles in question fly at

*PhD Candidate, Ann and H.J. Smead Department of Aerospace Engineering Sciences, University of Colorado Boulder, AIAA Student Member, connor.morency@gmail.com

†Professor, Ann and H.J. Smead Department of Aerospace Engineering Sciences, University of Colorado Boulder, AIAA Associate Fellow, kenneth.jansen@colorado.edu

hypersonic speeds. It is no secret that hypersonics are an integral part of the aviation world today. It then follows that many aviation scientists are working to uncover the secrets of this regime of flight and understand the complicated physics and chemistry contained within.

For many years the design of hypersonic flight vehicles was conducted mainly using empirical data with occasional analytical modeling. This method of engineering, which amounts to an educated guess and check system, is admittedly often effective in achieving acceptable designs. However, deep understanding of the flow physics is lacking when one relies on empirical data to guide design choices, and this reality has its pitfalls. It is advantageous to better understand the flow physics for two main reasons. First, it allows engineers to design better experiments informed by the flow physics such that optimization of the vehicle is achieved more efficiently with respect to both time and cost. And second, a more complete understanding of the underlying mechanisms present in complex physical processes allows for engineers to envision brand new systems inspired by the laws of nature instead of relying on anecdotal evidence from previous designs which can be limiting in terms of creativity. Furthermore, while analytical modeling can sometimes capture the full physics of relatively simple problems, this approach is infeasible for most flow problems of engineering interest that involve the complexities of thermochemical nonequilibrium. Herein lies the value of computational fluid dynamics (CFD) for hypersonic applications.

The hypersonic flight regime, when compared to subsonic and supersonic, is the most challenging and least understood area of research in the CFD community. A hypersonic flow is loosely defined by scientists and engineers as anything traveling at Mach 5 or above, but perhaps a more apt description, and one that hints at the true challenges of modeling these problems, is to say that hypersonic flow problems are high-enthalpy flow problems. This is because the enthalpy is high in all regions of the flow around a hypersonic vehicle. Before the shock, the high free-stream velocity drives up the enthalpy; after the shock, the enthalpy is buoyed by the high temperature. The post-shock region presents the greatest challenge with respect to physical modeling–this is where the thermochemical nonequilibrium effects reside. And the shock itself creates the most difficult problem with respect to solution convergence in a discretized method such as finite elements–the large discontinuities across a strong shock in hypersonic flow present grand challenges for residual-based solution finding methods.

Among the notable CFD codes that have paved the way for numerical simulation of thermochemical nonequilibrium flows are: University of Minnesota's US3D; University of Colorado's LeMANS*; NASA Langley's LAURA; NASA Ames' DPLR; and University of Texas' FIN-S. US3D [1] is a finite volume code that features implicit time-stepping, Steger-Warming vector splitting, non-catalytic or fully-catalytic wall boundary condition options, and a 5-species reacting flow solver based on Park's 1990 chemistry model [2]. LeMANS [3] is a finite volume code that can solve a 5-species, 8-species, or 11-species reacting flow formulation. It solves the viscous Jacobians in primitive form and the rest of the conservation equations in conservative form. It also features the ability to be coupled to a DSMC code for regions in the flow that do not qualify for the continuum assumption. LAURA and DPLR [4] are structured finite volume codes developed by NASA that have slightly different models for vibrational relaxation, electronic energy, and mass diffusion. FIN-S [5] is a finite element code that features a FANS-SA turbulence model, a radiative equilibrium wall boundary condition option, and adaptive meshing/shock fitting. Broadly speaking, in the last ten years there have been many research groups around the globe reporting new codes with similar capabilities to the few mentioned above.

The work presented in this document serves as an introduction to recent developments in PHASTA that have the potential to contribute to the growing field of research that is the simulation of hypersonic flows. These developments originate from the ideas discussed in [6]. PHASTA is designed to handle very computationally expensive problems–it is an efficient, massively parallel flow solver with the capability to handle problems on the scale of 92 billion elements and/or 3.1 million processes. Additionally, PHASTA features unique capabilities such as mesh adaptivity [7], scale resolving simulations such as detached eddy simulations [8], and flow control with jet actuators [9] that one day may be combined with the thermochemical nonequilibrium physics for novel research.

III. PHASTA

PHASTA (Parallel Hierarchic Adaptive Stabilized Transient Analysis) is a stabilized continuous-Galerkin finite element fluid solver that can solve the compressible Navier-Stokes equations. Since PHASTA is designed primarily for convection-dominated flows it uses the streamline upwind/Petrov-Galerkin (SUPG) finite element scheme to avoid the spurious node-to-node oscillations encountered when solving the Navier-Stokes equations with the Galerkin finite element scheme [10, 11]. PHASTA features different branches of the code that can solve the Navier-Stokes equations using distinct variable transformations that each offer unique advantages for certain problems. The branch that is

*Previously University of Michigan's.

the main subject of this research is the entropy variable branch that can solve ten conservation equations in total. The conservation laws of mass, momentum, vibrational energy, and energy that PHASTA solves expressed as partial differential equations are Equations 1, 2, 3, and 4, respectively:

$$(\rho_s)_{,t} + (\rho_s u_i)_{,i} = -(J_{si})_{,i} + \Omega_s \tag{1}$$

$$(\rho u_j)_{,t} + (\rho u_i u_j + P\delta_{ij})_{,i} = \tau_{ij,i} \tag{2}$$

$$(\rho e^v)_{,t} + (\rho u_i e^v)_{,i} = -(J_{si} e_s^v + q_i^v) + Q_{tr-v} + Q_{c-v} \tag{3}$$

$$(\rho e^{tot})_{,t} + (\rho u_i e^{tot})_{,i} + (u_i P)_{,i} = (u_j \tau_{ij} - q_i - q_i^v - J_{si} h_s)_{,i} \tag{4}$$

where Equation 1 can represent up to five equations (the subscript s can go from 1-5) and Equation 2 represents three equations, one for each spatial dimension. The ten conservation laws can subsequently be expressed in the conservative form as a single vector equation (Equation 5):

$$\mathbf{U}_{,t} + \mathbf{A}_i \mathbf{U}_{,i} - (\mathbf{K}_{ij}\mathbf{U}_{,j})_{,i} = \mathscr{F} \tag{5}$$

A change of interpolation variables can be performed on Equation 5 and the result is Equation 6:

$$\tilde{\mathbf{A}}_0 \mathbf{Y}_{,t} + \mathbf{A}_i \tilde{\mathbf{A}}_0 \mathbf{Y}_{,i} - (\mathbf{K}_{ij}\tilde{\mathbf{A}}_0 \mathbf{Y}_{,j})_{,i} = \mathscr{F}(\mathbf{U}(\mathbf{Y})) \tag{6}$$

where $\tilde{\mathbf{A}}_0 = \mathbf{U}_{,\mathbf{Y}}$ and is called the Reimannian metric tensor. More information about this matrix system and change of variables can be found in [6]. For the entropy variable branch, the vector-variable $\mathbf{Y}$ is Equation 7:

$$\mathbf{Y} = \frac{1}{T}\begin{bmatrix} \mu_s - \frac{u_k u_k}{2} \\ u_j \\ 1 - \frac{T}{T^v} \\ -1 \end{bmatrix} \tag{7}$$

The advantages of the entropy variable transformation are clearly outlined in [6] in which it is stated that the entropy variable formulation "expresses intrinsically the mathematical and physical stability provided by the second law of thermodynamics" and that "strong mathematical foundations support the analysis of convergence of finite element methods applied to the numerical solution" of Equation 6 expressed in terms of entropy variables. Most importantly, the entropy variable branch includes thermal and chemical nonequilibrium physics which will allow for the accurate simulation of hypersonic flows.

A second branch of PHASTA, the pressure-primitive formulation, has already been validated and verified for supersonic, turbulent flows [12]. The conservation laws of mass, momentum, and energy that PHASTA solves in this branch are Equations 8, 9, and 10, respectively:

$$(\rho)_{,t} + (\rho u_i)_{,i} = 0 \tag{8}$$

$$(\rho u_j)_{,t} + (\rho u_i u_j + P\delta_{ij})_{,i} = \tau_{ij,i} \tag{9}$$

$$(\rho e^{tot})_{,t} + (\rho u_i e^{tot})_{,i} + (u_i P)_{,i} = (u_j \tau_{ij} - q_i)_{,i} \tag{10}$$

For the pressure-primitive variable branch the vector-variable $\mathbf{Y}$ is Equation 11:

$$\mathbf{Y} = \begin{bmatrix} P \\ u_j \\ T \end{bmatrix} \tag{11}$$

The pressure-primitive variable formulation offers an advantage over the entropy variable formulation because it makes interpolation (with respect to the finite element method) easier. It is also easier to derive boundary conditions for the pressure-primitive formulation than for the entropy formulation. However, the pressure-primitive formulation lacks the thermochemical nonequilibrium capabilities present in the entropy formulation, making it unsuitable for the computation of hypersonic flows. It is used in this research for bench-marking purposes only.

Both branches of the code are designed for use with the Reynolds-averaged Navier-Stokes Spalart-Allmaras (RANS-SA) one-equation turbulence model [13], which provides an appropriate approximation of turbulence when used for steady-state applications. However, only the pressure-primitive formulation has been previously verified and validated for use with this model [14].

IV. Thermochemical Nonequilibrium Unit Tests

Three distinct features have been added to the entropy variable branch of PHASTA as part of this research that when used together enable the simulation of hypersonic flow with thermochemical nonequilibrium effects. These features are part of the conservation equations presented in Section III but are new and therefore require testing. The first new feature separates the translational-rotational and vibrational modes of temperature by introducing a second energy equation. The second new feature splits the mass conservation equation of a single species flow into five separate equations and, together with a chemistry solver, enables the solution of a five-species reacting flow. And third, a mass diffusion term is added to account for the diffusion of different species based on concentration gradients. Each new feature is discussed in the following Section along with a unit test that validates its implementation.

A. Vibrational Relaxation

The equation of state for the flow is derived under the assumption that the gas is a mixture of thermally perfect gases. Additionally, the rigid-rotator and harmonic-oscillator models are adopted for the atoms and diatoms in the gas [6]. With these facts in mind the species specific translational energy is Equation 12, the species specific rotational energy is Equation 13, and the species specific vibrational energy is Equation 14:

$$e_s^t = \frac{3}{2} R_s T \tag{12}$$

$$e_s^r = \begin{cases} 0 & \text{for atoms} \\ R_s T & \text{for diatoms} \end{cases} \tag{13}$$

$$e_s^v = \begin{cases} 0 & \text{for atoms} \\ \frac{R_s \theta_s^v}{\exp(\theta_s^v / T^v - 1)} & \text{for diatoms} \end{cases} \tag{14}$$

The sum of Equations 12, 13, and 14 represents the internal energy for each species. When temperatures reach around 11,400 K electronic excitation becomes significant for O_2 [6]. An equation similar in form to Equation 14 can be added to the system for electronic energy; however, this research is limited to hypersonic flight applications–temperatures are not expected to reach 11,400 K and therefore electronic energy is neglected. The source of vibrational energy due to collisional processes [15] is Equation 15:

$$Q_{tr-v} = \sum_{s=1}^{n} \rho_s \frac{e_{s*}^v - e_s^v}{\tau_s} \tag{15}$$

The species relaxation time τ_s is modeled using a Landau-Teller formulation [16] with coefficients provided by Millikan and White [17] and corrected for high temperatures according to Park [2]. It should be noted that the Millikan and White correlation and Park's high-temperature correction diverge from experimental data when used above 5000 K; therefore, the efficacy of this model likely begins to diminish above that temperature [18–20]. The unit test for vibrational relaxation compares an analytical solution to a one-dimensional flow computed by PHASTA for three single-species cases: O_2, NO, and N_2. It is assumed in the analytical model that the density is constant and that the temperature used in the relaxation time calculation is constant. In the PHASTA simulation the two temperatures, T and T^v, are set to be out of equilibrium at the inflow and then allowed to converge to the equilibrium temperature, T_*, as the flow advects through the domain (the process of which is driven by Equation 15). The prescribed inflow conditions for each PHASTA run are presented in Table 1; the conditions reflect a low supersonic flow (Mach < 1.5) at one atmosphere.

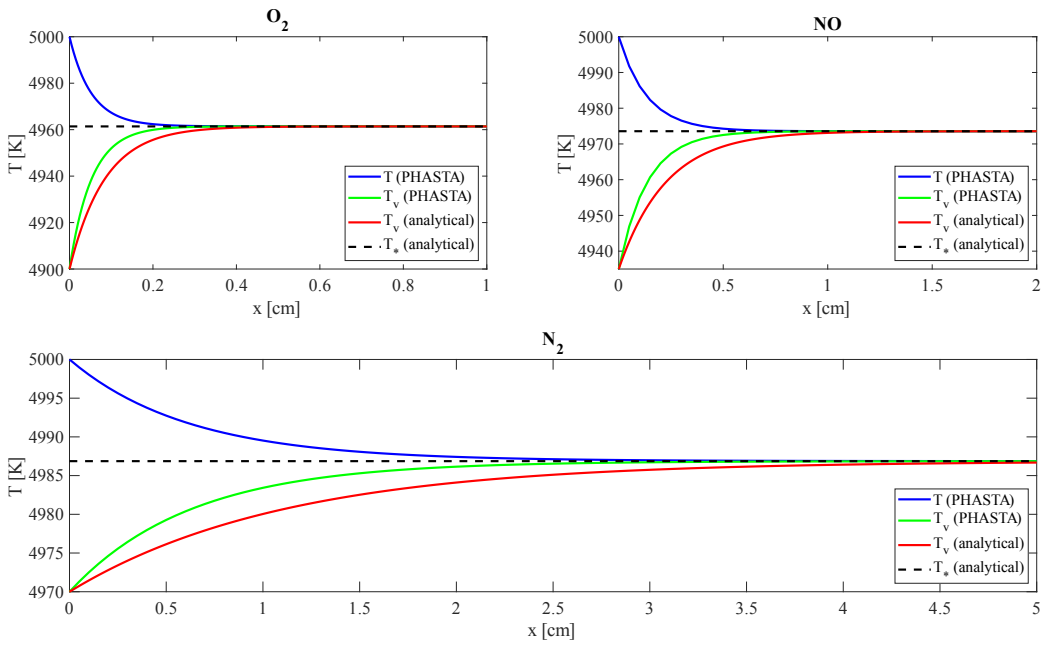

Fig. 1 Comparison of vibrational relaxation for O_2, NO, and N_2 molecules as computed by PHASTA and by an analytical model.

The temperatures are set to be around 5000 K because that is an appropriate condition at which to test the validity of the vibrational relaxation model [17]. The results of each unit test are displayed in Figure 1.

Table 1 Inflow details for the PHASTA portion of the vibrational relaxation unit test.

Inflow Parameter	O_2	NO	N_2
Vibrational Temperature	4900 K	4935 K	4970 K
Translational-rotational Temperature	5000 K		
Pressure	101325 Pa		
Velocity	1626 m/s		

The analytical model compares well with the PHASTA runs in Figure 1. Most importantly, both models predict the same equilibrium temperature and the curves follow similar paths to equilibrium. The relaxation behavior is not exactly the same between the simulation and the analytical model but this is expected due to the assumptions used when deriving the analytical model. In a real flow, the density and translational-rotational temperature will both change as the flow approaches thermal equilibrium which alters the relaxation time in space, which in turn will alter the path to equilibrium. Overall, Figure 1 gives confidence that the two-temperature model and vibrational relaxation model for diatomic molecules are correctly implemented in PHASTA.

B. Chemistry Model for Reacting Flow

When the temperature rises above 2000 K, as it often does under hypersonic conditions, the chemistry of the air begins to change due to dissociation and recombination [21]. Beyond 10,000 K ionization begins to take place [6]; however, this version of PHASTA is intended for hypersonic flight applications and will not be used to simulate flow at that high of a temperature. Thus, ionization is omitted from the model.

The air model used is an approximation of Earth's atmosphere and is comprised of 5 distinct species: N_2, O_2, NO, N, and O. Each species is assigned its own mass conservation equation (Equation 1). The species mass production rate due to chemical reactions, Ω_s, is Equation 16:

$$\Omega_s = M_s \dot{\omega}_s \tag{16}$$

where M_s is the species molar mass and $\dot{\omega}_s$ is the total rate of change in species concentration due to chemical reactions. $\dot{\omega}_s$ is calculated in part by use of the Arrhenius rate equation. The coefficients for the equilibrium constants used in the calculation of the reaction rates are provided by Park in [2]; there are 17 possible reactions in total. For brevity, a detailed description of these models is not shown here. If the reader is interested a complete derivation of $\dot{\omega}_s$ as implemented in PHASTA can be found in [22]. The computation of $\dot{\omega}_s$ is performed in PHASTA in a routine called the *chemistry module*.

A novel feature regarding the implementation of the chemistry module has been introduced. Instead of manually prescribing the mole fractions of each species in the domain (usually at the inflow and as an initial condition) as was originally suggested, the user must only prescribe the pressure and temperature. The equilibrium mole fractions are then computed from this condition using the chemistry module.

The process works as follows. First, the mole fractions are initialized for room temperature air: $\sim 79\%$ N_2, $\sim 21\%$ O_2, and trace amounts of the other constituents. The chemistry module is then run until the rate of change in species concentration is less than some tolerance, $|\dot{\omega}_s| < tol$, for each species; the exact tolerance can be adjusted by the user but the default is $tol = 10^{-5}$. As the module is run, the pressure is constantly recomputed using the new mole fractions such that the ideal gas law is satisfied for each species. The final equilibrium mole fractions and pressure are then set as the new inflow and initial conditions. This feature ensures that the inflow and initial conditions are reflective of a system that is in equilibrium before the PHASTA solver begins to advance in time, without the user having to worry about manually computing the equilibrium conditions which would introduce the possibility of user error. That being said, the chemistry module is activated only at temperatures of 2000 K and above [6]. This means that for many flow problems of interest where the inflow and initial temperatures are set below 2000 K the corresponding mole fractions will be equivalent to those at room temperature.

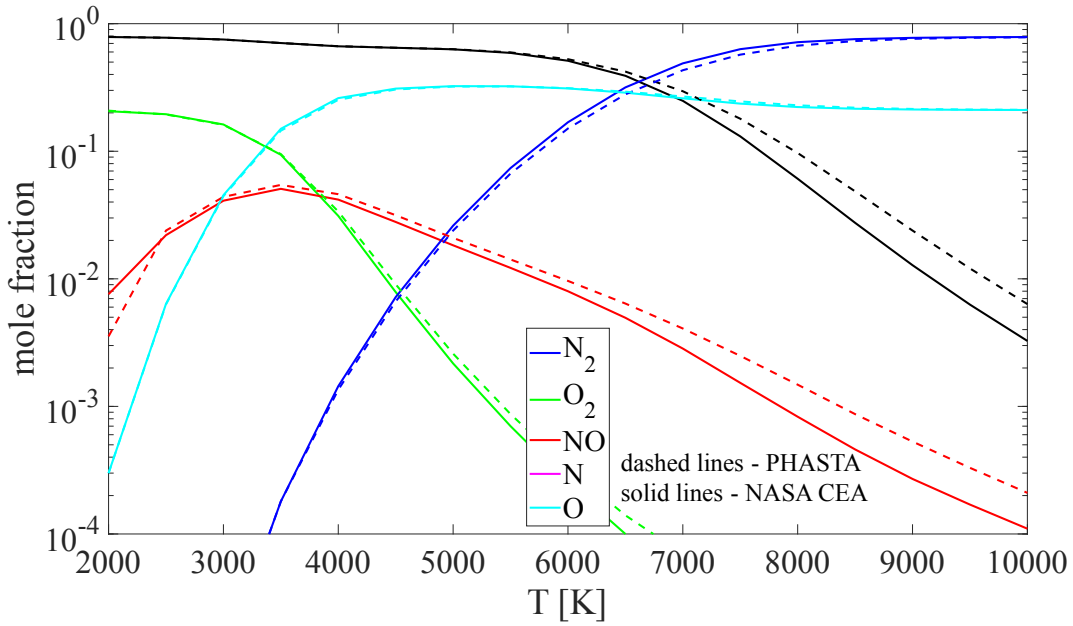

Fig. 2 Equilibrium mole fractions for 5-species air as computed by PHASTA and by NASA CEA.

The unit test for the chemistry module compares the equilibrium mole fractions as computed by PHASTA and by the NASA CEA (chemical equilibrium with applications) code [23] from 2000 K to 10,000 K at intervals of 500 K. According to [24], "CEA remains the gold standard for detailed analysis of problems involving combustion, rocketry, shock and detonation". Importantly, the CEA code is designed to calculate equilibrium mole fractions only and therefore cannot be adopted into a non-equilibrium code such as PHASTA. It is, however, quite useful as a comparison tool in this context.

As shown in Figure 2, PHASTA compares well with NASA CEA. For N and O the codes predict similar mole fractions across the entire temperature range. For N_2, O_2, and NO the codes compare well at low temperatures but increasingly differ after around 5000 K. It is important to note the log scale on the y-axis of the plot–differences in the mole fraction of N_2 at high temperatures appear small, for example, when in fact those differences cause a much more drastic change in the flow physics than the visually larger differences in the mole fraction of NO that are actually orders of magnitude smaller.

It is expected that PHASTA does not exactly match NASA CEA. It has been previously reported that Park's model for the Zeldovich (or "neutral exchange") reactions begins to diverge from experimental data above 5000 K [25]. However, given the limitations of the Park model the performance is as expected and this unit test gives confidence that the chemistry model is correctly implemented and can be used for hypersonic flight calculations.

C. Mass Diffusion

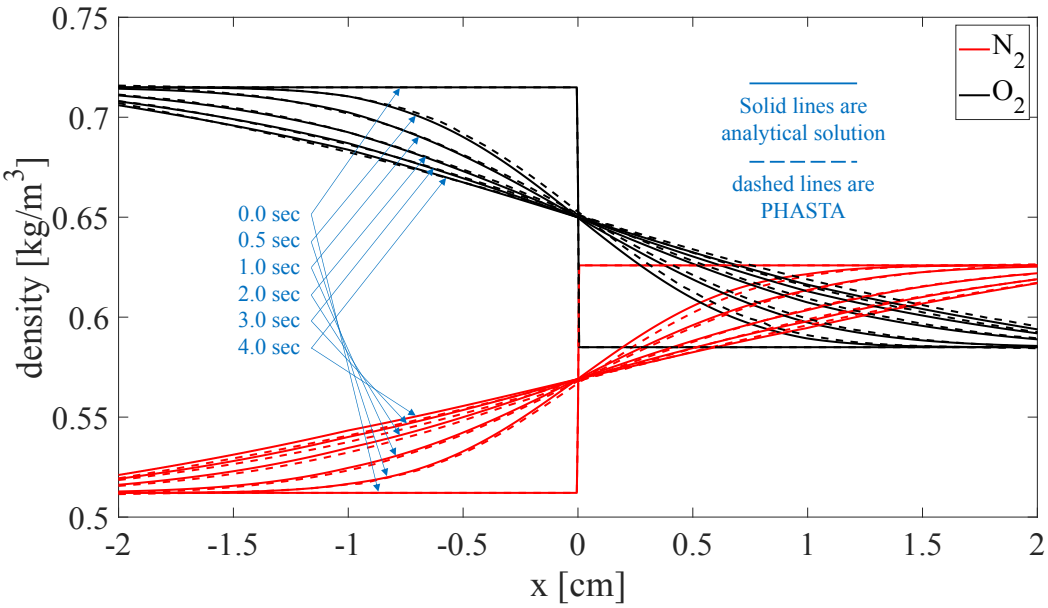

Fig. 3 Diffusion of N_2 and O_2 as computed with PHASTA and with an analytical model (direct integration of Fick's law).

When multiple species of a gas mixture are present, each individual species will tend to move from a region of higher species concentration to a region of lower species concentration. This process is driven by a gradient in Gibbs free energy and is called mass diffusion. Mass diffusion can occur across regions even if the total density in each region is the same since it is based on the gradient of each individual species concentration (not the gradient of total density). The diffusion mass flux, J_{si}, is calculated using Fick's law and is Equation 17:

$$J_{si} = -\rho D \frac{\partial x_s}{\partial x_i} \tag{17}$$

The diffusion coefficient D is given by Equation 18:

$$D = \frac{\kappa_{tr} Le}{\rho C_p^{tr}} \tag{18}$$

The diffusion coefficient is the same for all species–this approach is referred to as the constant Lewis number (CLN) method. The Lewis number Le is set to 1.4 in PHASTA. The CLN method "works well as long as the majority of the molecules of the flow have similar diffusion properties, for instance the nitrogen and oxygen molecule in air" [26]. Also presented in [26] is that the CLN method compares well with other more comprehensive (multi-component) mass diffusion methods up to a velocity of about 8000 m/s, above which the CLN method begins to diverge from the other

methods. This suggests that the CLN method is suitable for hypersonic flight applications but not for hypersonic reentry applications.

The unit test for mass diffusion compares a one-dimensional integration of Fick's law in MATLAB to a one-dimensional simulation in PHASTA. Both MATLAB and PHASTA are given identical initial conditions. A domain of length 4 cm is split in half such that one side starts with 45% N_2 and 55% O_2 and the other side starts with 55% N_2 and 45% O_2 (the percentages refer to molar concentrations). The initial pressure is 101325 Pa, the initial temperature is 300 K, and the initial velocity is 0 m/s. MATLAB and PHASTA then advance in time and the species diffuse across the center of the domain. The results are shown in Figure 3.

PHASTA shows good agreement with the isolated integration of Fick's law. Figure 3 clearly shows that the added mass diffusion term in PHASTA is driving the flow toward an equilibrium state. The species densities from the PHASTA simulation at each time increment closely match those computed by the integration of Fick's law. It is not expected for the solutions to exactly match because the PHASTA simulation accounts for other gradients in the flow such as density, temperature, and velocity. Overall, Figure 3 gives confidence that the mass diffusion term is correctly implemented in PHASTA.

V. Turbulent Supersonic Flat Plate

Validating the five-species, two-temperature entropy variable formulation in PHASTA requires more than just unit tests. Canonical flow problems should first be solved with the entropy variable formulation of PHASTA to show that the code is performing as expected before more challenging problems–such as those featuring strong shocks–are tackled with the new hypersonic flow solver. One such canonical problem is turbulent supersonic flow over a flat plate. Since the pressure-primitive version of PHASTA has already been verified and validated for this type of problem [12] the results it produces can be used as the standard to which the entropy code should perform. If the two codes produce results within an acceptable margin of error given identical boundary conditions and initial conditions, it can be concluded that the entropy formulation of PHASTA is also suitable for use with problems that include supersonic turbulent boundary layers. While preliminary simulations have been performed, grid refinement studies are required to complete this study. The following discussion describes simulations that were run on a coarse mesh–it serves as a progress update, not a validation study.

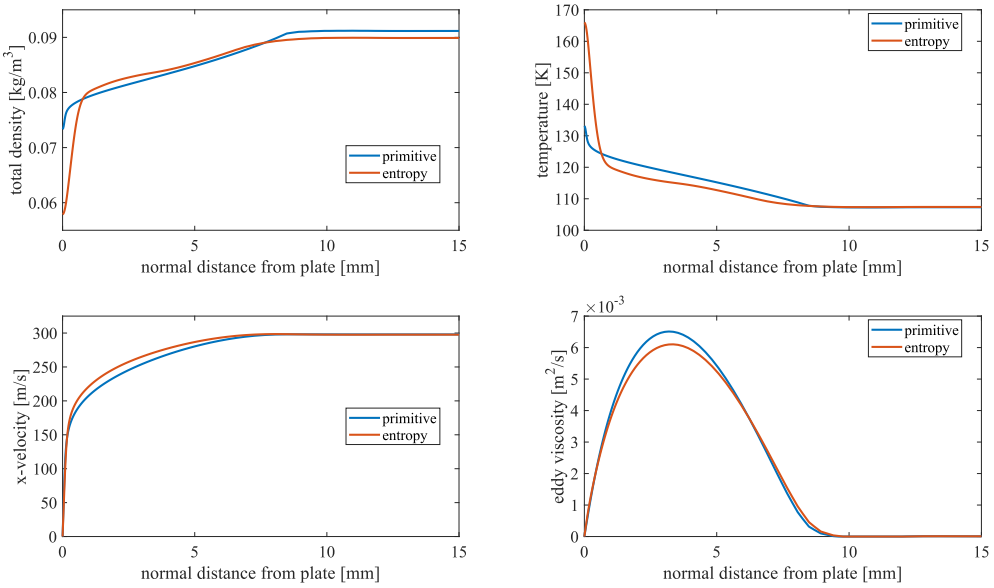

Fig. 4 Total density, temperature, x-velocity, and eddy viscosity boundary layer profiles for pressure-primitive and entropy variables taken at x = 0.05 m from the inflow.

The simulation is designed as simply as possible to reduce computational expense. First, a boundary layer profile

is taken from a turbulent supersonic flat plate simulation that was previously completed using the pressure-primitive formulation of PHASTA. This profile includes solution values such as temperature, pressure, velocity, and the RANS eddy viscosity (Spalart-Allmaras variable). This profile is set as the inflow condition for both the pressure-primitive and entropy variable simulations. The simulations are then executed with identical boundary conditions elsewhere, such as zero heat flux and the no-slip condition enforced on the plate. Boundary layer profiles can then be extracted from each simulation at an identical location on the plate and the results can be compared. In this case, the profiles were taken at x = 0.05 m from the inflow. The boundary layer profiles for each simulation are shown in Figure 4. Boundary layer integral quantities for each simulation are shown in Table 2.

Table 2 Boundary layer quantities for the entropy and pressure-primitive formulations with percent difference.

Parameter	Pressure-primitive	Entropy
θ [mm]	1.04	1.06 (+1.9%)
δ^* [mm]	2.41	2.46 (+2.0%)
$H = \frac{\theta}{\delta^*}$	2.32	2.33 (+0.43%)
u_τ [m/s]	13.0	13.1 (+0.76%)
C_f	2.20×10^{-3}	2.25×10^{-3} (+2.2%)

As can be seen in Figure 4, the velocity and eddy viscosity profiles compare fairly well (some discrepancy) between the two variable formulations. However, the density and temperature profiles do not compare as favorably, especially near the wall. As shown in Table 2, the momentum thickness θ and the displacement thickness δ^* show differences between the variable formulations on the order of fifteen to twenty percent. The reason for these discrepancies is still under investigation as they are far larger than expected. There is suspicion that there may be a bug in the code somewhere that is causing the temperature to creep up and the density to creep down at the wall. However, the mesh used for these simulations is too coarse for any concrete conclusions to be drawn. Further investigation, starting with a grid refinement study, is required.

While there are clearly still problems to be sorted out with the entropy variable formulation of the code, there are encouraging signs. For example, the free-stream values (15 mm from the plate as can be seen in Figure 4) show good agreement between the codes. The Eddy viscosity calculations show similar behavior throughout the boundary layer, which suggests that the turbulence model is correctly implemented in the entropy code (this is not validated yet however). From Table 2, it can be seen that the ratios between the integral quantities show good agreement. This suggests that if there is an error in the code, it scales with the density and not the velocity which is consistent with the profiles shown in Figure 4. Overall, the code shows promise that it will soon be able to correctly predict supersonic turbulent boundary layers; however, there is still work to be done to achieve this goal.

VI. Conclusion

This document serves as an introduction and benchmark study for the PHASTA hypersonic CFD code. The code formulation was described in Section III, unit tests validating certain nonequilibrium features were performed in Section IV, and preliminary results for a turbulent supersonic flat plate simulation were discussed in Section V. The new features–namely the two-temperature model, reacting flow capabilities, mass diffusion, and the RANS turbulence model–seem to be performing as expected. However, the entropy variable formulation with thermochemical nonequilibrium capabilities still requires further development before it can be confidently used to simulate flows of engineering interest.

Acknowledgments

Connor W. Morency's research for this Paper was conducted with U.S. Government support and awarded by the Department of Defense, Office of Naval Research, National Defense Science and Engineering Graduate Fellowship. The authors gratefully acknowledge Simmetrix, Inc., for its meshing and geometric modeling libraries, Altair Engineering for its linear algebra solver library, and Kitware for its visualization tools. Lastly, the authors thank the Scientific Computation Research Center (SCOREC) at Rensselaer Polytechnic Institute (RPI) for its core mesh partitioning tools, supported by the U.S. Department of Energy, Office of Science, Office of Advanced Scientific Computing Research,

under award DE-SC00066117 (FASTMath SciDAC Institute).

References

[1] Nompelis, I., "Computational Study of Hypersonic Double-Cone Experiments for Code Validation," doctoral thesis, University of Minnesota, 2004.

[2] Park, C., *Nonequilibrium Hypersonic Aerothermodynamics*, Wiley, 1990.

[3] Scalabrin, L. C., "Numerical Simulation of Weakly Ionized Hypersonic Flow Over Reentry Capsules," doctoral thesis, University of Michigan, 2007.

[4] Hash, D., Olejniczak, J., Wright, M., Prabhu, D., Pulsonetti, M., Hollis, B., Gnoffo, P., Barnhardt, M., Nompelis, I., and Candler, G., *FIRE II Calculations for Hypersonic Nonequilibrium Aerothermodynamics Code Verification: DPLR, LAURA, and US3D*, 2007. https://doi.org/10.2514/6.2007-605.

[5] Kirk, B. S., Stogner, R. H., Bauman, P. T., and Oliver, T. A., "Modeling hypersonic entry with the fully-implicit Navier–Stokes (FIN-S) stabilized finite element flow solver," *Computers & Fluids*, Vol. 92, 2014, pp. 281–292. https://doi.org/https://doi.org/10.1016/j.compfluid.2013.10.003.

[6] Chalot, F., Hughes, T., and Shakib, F., "Symmetrization of conservation laws with entropy for high-temperature hypersonic computations," *Computing Systems in Engineering*, Vol. 1, No. 2, 1990, pp. 495–521. https://doi.org/https://doi.org/10.1016/0956-0521(90)90032-G, computational Technology for Flight Vehicles.

[7] Fang, J., Pruser, M. K., Smith, C., Balakrishnan, R., Bolotnov, I. A., and Jansen, K. E., "Annular Flow Simulation Supported by Iterative In-Memory Mesh Adaptation," *Nuclear Science and Engineering*, Vol. 194, No. 8-9, 2020, pp. 676–689. https://doi.org/10.1080/00295639.2020.1743577.

[8] Tejada-Martínez, A. E., and Jansen, K. E., "Spatial test filters for dynamic model large-eddy simulation with finite elements," *Communications in Numerical Methods in Engineering*, Vol. 19, No. 3, 2003, pp. 205–213. https://doi.org/https://doi.org/10.1002/cnm.509.

[9] Jansen, K. E., Rasquin, M., Farnsworth, J. A., Rathay, N., Monastero, M. C., and Amitay, M., "Interaction of a Synthetic Jet with Separated Flow over a Vertical Tail," *AIAA Journal*, Vol. 56, No. 7, 2018, pp. 2653–2668. https://doi.org/10.2514/1.J056751.

[10] Brooks, A. N., and Hughes, T. J., "Streamline upwind/Petrov-Galerkin formulations for convection dominated flows with particular emphasis on the incompressible Navier-Stokes equations," *Computer Methods in Applied Mechanics and Engineering*, Vol. 32, No. 1, 1982, pp. 199–259. https://doi.org/10.1016/0045-7825(82)90071-8.

[11] Hughes, T., Scovazzi, G., and Tezduyar, T., "Stabilized Methods for Compressible Flows," *Journal of Scientific Computing*, Vol. 43, 2010, pp. 343–368. https://doi.org/10.1007/s10915-008-9233-5.

[12] Morency, C. W., and Jansen, K. E., *Shock Stand-Off Distance and Development of a Supersonic Turbulent Boundary Layer: CFD Analysis of a Diamond-shaped 2D Fin*, 2023. https://doi.org/10.2514/6.2023-3016.

[13] Spalart, P., and Allmaras, S., *A one-equation turbulence model for aerodynamic flows*, 1992. https://doi.org/10.2514/6.1992-439.

[14] Jansen, K. E., Whiting, C. H., and Hulbert, G. M., "A generalized-α method for integrating the filtered Navier–Stokes equations with a stabilized finite element method," *Computer Methods in Applied Mechanics and Engineering*, Vol. 190, No. 3, 2000, pp. 305–319. https://doi.org/10.1016/S0045-7825(00)00203-6.

[15] Vincenti, G., and Kruger, C., *Introduction to Physical Gas Dynamics*, Wiley, 1986.

[16] Lee, J.-H., *Basic governing equations for the flight regimes of aeroassisted orbital transfer vehicles*, 1984. https://doi.org/10.2514/6.1984-1729.

[17] Millikan, R. C., and White, D. R., "Systematics of Vibrational Relaxation," *The Journal of Chemical Physics*, Vol. 39, No. 12, 1963, pp. 3209–3213. https://doi.org/10.1063/1.1734182.

[18] Streicher, J. W., Krish, A., and Hanson, R. K., "High-temperature vibrational relaxation and decomposition of shock-heated nitric oxide. I. Argon dilution from 2200 to 8700 K," *Physics of Fluids*, Vol. 34, No. 11, 2022, p. 116122. https://doi.org/10.1063/5.0109109.

[19] Streicher, J. W., Krish, A., and Hanson, R. K., "High-temperature vibrational relaxation and decomposition of shock-heated nitric oxide: II. Nitrogen dilution from 1900 to 8200 K," *Physics of Fluids*, Vol. 34, No. 11, 2022, p. 116123. https://doi.org/10.1063/5.0122787.

[20] Streicher, J. W., Krish, A., and Hanson, R. K., "Coupled vibration-dissociation time-histories and rate measurements in shock-heated, nondilute O2 and O2–Ar mixtures from 6000 to 14 000 K," *Physics of Fluids*, Vol. 33, No. 5, 2021, p. 056107. https://doi.org/10.1063/5.0048059.

[21] Anderson, J., *Hypersonic and High Temperature Gas Dynamics Second Edition*, AIAA, Inc., 2006.

[22] Pointer, J., "Influence of Interpolation Variables and Discontinuity Capturing Operators on Inviscid Hypersonic Flow Simulations Using a Stabilized Continuous Galerkin Solver," doctoral thesis, University of Colorado, 2022.

[23] Gordon, S., and McBride, B., "Computer Program for Calculation of Complex Chemical Equilibrium Compositions and Applications," *NASA Reference Publication 1311*, 1996.

[24] "Introduction to CEA," https://cearun.grc.nasa.gov/intro.html, 2023.

[25] Streicher, J. W., Krish, A., and Hanson, R. K., "Laser absorption study of the N2 + O $\rightarrow$ NO + N and NO + O $\rightarrow$ O2 + N Zeldovich reactions in shock-heated N2O mixtures," *Physics of Fluids*, Vol. 35, No. 4, 2023, p. 046119. https://doi.org/10.1063/5.0147764.

[26] Gosse, R., and Candler, G., *Diffusion Flux Modeling: Application to Direct Entry Problems*, 2005. https://doi.org/10.2514/6.2005-389.